Radiation Physics and Chemistry 115 (2015) 43–48

Contents lists available at ScienceDirect

Radiation Physics and Chemistry

journal homepage: www.elsevier.com/locate/radphyschem

# Preparation and characterization of a novel ionizing electromagnetic radiation shielding material: Hematite filled polyester based composites

E. Eren Belgin [a,*], G.A. Aycik [a], A. Kalemtas [b], A. Pelit [a], D.A. Dilek [a], M.T. Kavak [a]

[a] Mugla Sitki Koçman University, Faculty of Science, Department of Chemistry, Mugla 48000, Turkey
[b] Bursa Technical University, Faculty of Natural Sciences, Architecture and, Engineering, Department of Department of Metallurgical and Materials Engineering, Osmangazi, Bursa 16190, Turkey

## HIGHLIGHTS

- Isophytalitic polyester-natural mineral (hematite) filled composites were prepared.
- Ionizing electromagnetic radiation shielding performances were investigated.
- Density evaluation and microscopic studies were carried out.
- Attenuation coefficients were determined for different energies.
- The mass attenuation coefficients reached 98% of the elemental lead.

## ARTICLE INFO

*Article history:*
Received 18 March 2015
Accepted 3 June 2015
Available online 8 June 2015

*Keywords:*
Ionizing electromagnetic radiation
Radiation shielding
Composite shielding
Polymer composite
Hematite

## ABSTRACT

Isophthalic polyester (PES) based and natural mineral (hematite) filled composites were prepared and characterized for ionizing electromagnetic radiation shielding applications. Density evaluation and microscopic studies of the composites were carried out. Shielding performances of the composites were investigated for three different IEMR energy regions as low, intermediate and high. The mass attenuation coefficient of the prepared composites reached 98% of the elemental lead. In addition, the studied composites were superior to lead by virtue of their non-toxic nature.



## 1. Introduction

Gamma and X rays are ionizing electromagnetic radiation (IEMR) types and they have high enough energy to ionize atoms of the interacting matter. Penetrating ability of IEMR is high in material since it is massless and uncharged. Thus, appropriate shielding materials must be used to protect humans and the environment from the harmful effects of IEMR. Shielding materials reduce the exposure dose by interacting with the radiation itself and reducing its intensity. At the present time, high density materials such as lead bricks, high density concrete and such other metal based shielding materials as tungsten, copper, bismuth and steel are used as shielding materials. Lead is the most widely used shielding material because of its high density, high atomic number and cost efficiency. However, lead has significant disadvantages like high toxicity and heaviness, and low mechanical and chemical stability limit its application areas and usage.

In the modern era improvement of new shielding materials is highly necessary. Composite materials prepared by using several matrix and filler materials are one type of studied shielding materials. Polymers are one of the favorite matrix materials used for IEMR shielding composites because of their light weight. Polymer-bismuth (Plionis et al., 2009), lead-natural rubber (Gwaily and Madani, 2002; Mheemeed et al., 2011) and lead-unsaturated polyester composites are some of studied polymer based composites for radiation shielding. There are also some studies in which several natural minerals are used as filler materials for the composite IEMR shielding. One of these studies was about hematite–serpentine and ilmenite–limonite filled cements for neutron and gamma shielding applications. In the study, total flux was calculated by analytical methods and by using a scintillation detector then the high agreement between experimental and theoretical results was reported (Bashter et al., 1996). The same composites

* Corresponding author.
*E-mail address:* ebelgin@mu.edu.tr (E. Eren Belgin).

http://dx.doi.org/10.1016/j.radphyschem.2015.06.008
0969-806X/

were also investigated as reactor biological shields in another study (Kansouh, 2012). In the study, serpentine–cement composites were reported as much more suitable shielding materials for gamma shielding and ilmenite–limonite–cement composites are reported as more suitable for reactor biological shielding. A comprehensive literature review revealed that the potential IEMR shielding properties of natural mineral filled composites were investigated only with cement matrixes. Thus mineral–polymer composites and their shielding properties at different IEMR energy regions have not been exploited so far.

## 2. Theory

In the present study, we attempted to prepare and characterize the isophthalic unsaturated polyester (PES) based and hematite (natural iron mineral) filled composites for IEMR shielding applications. The role of hematite was increasing the IEMR shielding performance of the composite while the role of polymer matrix was providing load–stress transfer and giving easy formability and processability to the composite. PES was chosen as the matrix polymer because of its low density, good strength/density ratio, and low cost of raw material and production. In addition, thanks to the hydrogen content of the polymer generating many interaction points in the polymer and due to the lack of heavier atoms than carbon in the polymer minimum formation of secondary radiation is possible.

The shielding properties of the composites were investigated for three different IEMR energy regions as low, intermediate and high energies since interaction mechanisms of IEMR with matter differs mainly according to IEMR energy. The predominant interaction process for the low IEMR energy region is the photoelectric effect that first falls off rapidly then more slowly with increasing energy for photon energies above the K-binding energy of the absorber material. The photoelectric effect is approximately proportional to $Z^5$ where Z represents the atomic number of the absorber material. When the IEMR energy rises the Compton effect becomes the process responsible for energy loss. The Compton scattering per electron is nearly independent of Z and therefore the scattering coefficient per atom is proportional to Z. The last of the energy loss processes is pair production, which cannot occur when IEMR energy is less than 1.02 MeV. Thus it is the predominant process at high energy region and is proportional to $Z^2$ (Friedlander et al., 1981).

## 3. Experimental

### 3.1. Constituents of the composites and preliminaries for production

PES that is a thermoset polymer with a density of 1.15 g $cm^{-3}$ and low volumetric shrinkage was used as the matrix material of the composites. PES was procured commercially as PES resin in styrene monomer.

The hematite with a density of 5.26 g $cm^{-3}$and trigonal crystal structure was procured commercially as middle sized stones. The hematite mineral stones were crushed, homogenized and sieved to $<5$ μm particle size after oven drying to the constant weight at 110 °C temperature. The exact constituents of the mineral were revealed by performing X-ray fluorescens analysis and it was determined that approximately 86% of the hematite mineral was $Fe_2O_3$ and residuals consisted of several impurities (Table 1).

Particle size and distribution analysis was also performed for prepared hematite filler and it was determined that 90% of the particles had particle size below 4.6 μm, 50% had particle size below 1.3 μm and 10% of them had particle size below 0.5 μm.

**Table 1**
Constituents of hematite used in the study determined by XRF analysis.

| Consistuent | w/w Content (%) | Detection limit (%) | Consistuent | w/w Content (%) | Detection limit (%) |
|---|---|---|---|---|---|
| MgO | 1.2552 | 0.0553 | $TiO_2$ | 0.2090 | 0.0212 |
| $Al_2O_3$ | 1.5064 | 0.0395 | $Cr_2O_3$ | 0.0646 | 0.0114 |
| $SiO_2$ | 6.0783 | 0.026 | MnO | 0.0932 | 0.011 |
| $P_2O_5$ | 0.1439 | 0.0075 | $Fe_2O_3$ | 85.7641 | 0.0606 |
| $SO_3$ | 0.2489 | 0.0121 | NiO | 0.2040 | 0.0081 |
| $K_2O$ | 0.4299 | 0.0095 | CuO | 0.0467 | 0.007 |
| CaO | 0.7058 | 0.0123 | A.Z. | 3.2500 | |

### 3.2. Preparation of the composites

Free radicalic polymerization process was performed for PES resin for formation of crosslinks that would lead to a rigid three dimensional lattice of the PES thermoset. Methyl ethyl ketone peroxide (MEKP) was used as the radical source with cobalt octoate (Coct) catalyst in the polymerization process. The composites were prepared with five different filler loadings between 10% and 50%. Filler particles were dispersed into the resin with a mechanical blender at 120 rpm after weighing of the filler and matrix material with a calibrated ($10^{-3}$ g) electrical balance. Then 0.75% Coct and 1.25% MEKP were dispersed into the resin by mechanical mixing and the crosslinking process was started in the resin. The mixing was continued until gelation point to avoid any precipitation of the filler particles in the PES resin and then the mixture was placed in a double sided closed steelmold. The composites were cured in the mold for 24 h at room temperature and 8 h at 80 °C constant temperature.

### 3.3. Characterization of composites

#### 3.3.1. Density evaluation and structure of the composites

Experimental densities of the composites were evaluated using Archimedes' density measurement equipment (Kirdsiri et al., 2009). Theoretical values of the bulk densities of the composites were also calculated (Harish et al., 2008) and compared with the experimental values. The FTIR analysis of the composites was also performed to understand the nature of interaction between PES and filler particles. The fractured and polished surfaces of the composites were examined under a scanning electron microscope for morphological examination of the composites in order to understand dispersibility of hematite with polymer matrix, microstructure of the composites, and binding behavior between the filler particles and polymer matrix.

#### 3.3.2. IEMR attenuation performance measurements

The IEMR attenuation performance measurements were performed using a gamma spectrometer with a 110 $cm^3$ well-type HPGe detector coupled with a 64 k channel analyzer. The system had a resolution of 3.78 keV at 1.33 MeV gamma-ray peak of Co-60. The detector was housed in lead shielding 10 cm thick, lined with 1.5 mm thick tin and 1.0 mm thick copper in order to reduce the X-ray interference. The IEMR attenuation measurements were carried out on the basis of a standard mixed point gamma-source containing Am-241, Cd-109, Co-57, Ce-139, Sn-113, Cs-137, Y-88 and Co-60 radionuclides that had photopeaks at 60, 88, 122, 166, 392, 662, 898, 1173, 1333, 1836 keV energies. These radionuclide photopeak energies were preferred for measurements because of being single, clear and having relatively high emission probabilities. Dispersion of the photopeak energies of the radionuclides between 60 and 1836 keV permitted an attenuation performance measurement for different energy ranges. In IEMR attenuation performance measurement studies, a cylindrical lead shield,

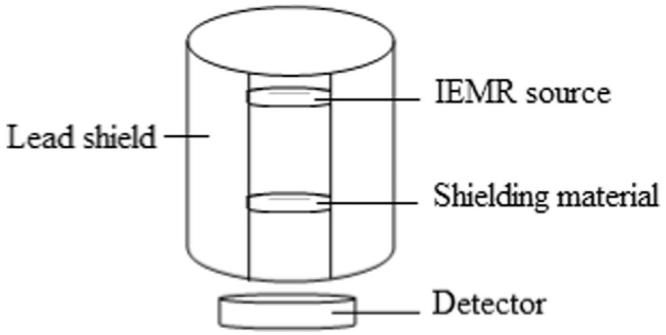


**Fig. 1.** Geometrical arrangement of the IEMR attenuation performance measurement system.

placed onto the detector with a well hole was used for the measurements by allowing the detector to count only the gamma rays coming through the shielding material by blocking the gamma rays coming through to the detector from other directions. Then the radionuclide source was placed on this lead shield and shielding materials were placed into the lead shield between IEMR source and detector (Fig. 1).

All the performance calculations were done relatively by comparing initial and residual intensities of the radionuclide source to avoid any efficiency calibration errors of the detector. Initial intensity of the radioactive source was measured without placing any other material between the source and detector. The same measurements were made for prepared composites and elemental lead by using the same geometrical arrangement to compare residual intensity (attenuation performances) of the elemental lead with prepared composites. The data acquisitions were performed for a period of 6000 s that gave $<1\%$ count error. All measurements were done three times and the determined mean values were used for the calculations.

*3.3.3. Linear and mass attenuation coefficient calculations*

A beam of IEMR with initial intensity of $I_0$ will have residual intensity of $I$ after traversing the material. This relation is given by Eq. (1) where $\mu_L$ is the total linear attenuation coefficient of the material ($cm^{-1}$) for IEMR with known energy and $x$ is thickness of the absorbing material.

$$I = I_0 \exp(-\mu_L x) \tag{1}$$

In the study, intensities (the number of counts per second) recorded by the detector for the radioactive source, the source+composites and the source+elemental lead were calculated by using manually selected net areas under thedetected photopeaks of the radionuclides of the mixed source via Maestro-Ortec software of the detector. The $\mu_L$ values of the prepared composites and elemental lead were then calculated via Eq. (1) after determination of $I_0$ and $I$ values.

Mass attenuation coefficient ($\mu_M$) of a material is another way to express attenuation property of the material and it is independent of actual density and physical state of the material. After evaluating $\mu_L$ values, $\mu_M$ values of the composites were determined by dividing $\mu_L$ value with density ($\rho$) of the material.

*3.3.4. Half value layer calculations*

Half value layer (HVL) is described as the thickness of the material at which the intensity of the radiation after interacting with the absorber material is reduced to half of its energy before interaction. HVL (cm) is given with Eq. (2).

$$\mathrm{HVL} = 0.693/\mu_L \tag{2}$$

In the study, the HVL values of the shielding materials were calculated via Eq. (2) after calculation of $\mu_L$ values.

## 4. Results and discussions

*4.1. Density and microstructure of the composites*

The experimental and theoretical densities were determined and composite designations, filler loading percentages and densities of the prepared composites are summarized in Table 2.

When the heavy filler loading of the composite material increases that means an increment in the Z number and density of the composite material (Plionis et al., 2009). Thus, in the study dispersion of the high density filler materials with the low density matrix caused an increment in the density of the composites, as is expected. The densities of the composites were observed to increase with increasing filler loading and the experimental and theoretical densities were observed in good agreement (Fig. 2). The maximum filler loading of 50% caused an increment in the density of the composite matrix of approximately 40%.

Increasing behavior of Fig. 2 curve also confirmed that the studied filler loading percentages were below the critical filler loading values. Above the critical filler loadings there might not be enough polymer to cover all the filler surface that would lead to an increment in free volume of the composite and a decrement in the density of the composite (Harish et al., 2008).

The micrographs determined by SEM studies for the polished (a, b) and fractured (c, d) surfaces of the HPES-50 are shown in Fig. 3.

The most important requirement for the composites was homogeneous dispersion of filler particles with minimal coagulation and in Fig. 3a good dispersibility of the filler particles was observed within the polymer matrix at the polished surface of the composite. Energy dispersive X-ray analysis (EDS) was also carried out for polished surface of the composite for elemental analysis of the different regions and results are given in Table 3.

The EDS results showed that the dark regions (b1) shown in Fig. 3 are a matrix of the composite that is mostly composed of carbon and oxygen. The light regions (b2) were the $Fe_3O_4$ filler particles that were a major constituent of the hematite. The middle light regions (b3) were the other impurities that were minor constituents of the hematite. The palladium content of the regions was caused by the coating of the SEM samples. After EDS analysis of the composite EDS mapping studies were also done for the polished surface and the homogeneous dispersion of the

**Table 2**
Sample designations, filler loading percentages and experimental/theoretical densities of the prepared composites.

| Sample designation | Filler concentration of composite (%) | Experimental density (g $cm^{-3}$) | Theoretical density (g $cm^{-3}$) |
|---|---|---|---|
| HPES-10 | 10 | 1.32 | 1.25 |
| HPES-20 | 20 | 1.43 | 1.36 |
| HPES-30 | 30 | 1.56 | 1.50 |
| HPES-40 | 40 | 1.73 | 1.67 |
| HPES-50 | 50 | 1.93 | 1.89 |

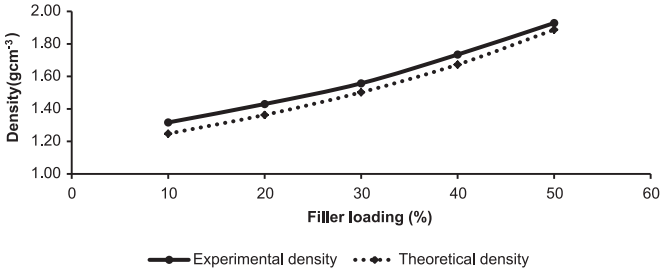


**Fig. 2.** Variation of the theoretical and experimental values of densities with respect to filler loading.

elements was confirmed.

In Fig. 3c, the SEM micrographs of the fractured surfaces of the composite are given and the homogeneous dispersion of filler particles within the matrix can be seen. On the fractured surface, there were not many filler particle holes that could take shape in the fracture instant because of poor adhesion between matrix and filler particles (El-Sarraf and El-Sayed Abdo, 2013). At some confined areas of the fractured surface (d1 and d2), coagulated filler particles had poor adhesion and surrounding holes were seen when the magnitude was enlarged that could be avoided by surface treatment of the filler particles.

The FTIR spectrums of the composite matrix PES (a) and HPES-50 (b) are given in Fig. 4.

The FTIR spectrum of PES showed absorption bands corresponding to the C–H bonds and C=O bonds at 2962 $cm^{-1}$ and 1719 $cm^{-1}$, respectively (Settle, 1997). The FTIR spectrum of 50% hematite filled composite HPES-50 was also in good agreement with pure PES as shown in Fig. 4. Thus it was thought that by the addition of the filler the functional group intensity of the PES was not changed since there was no chemical interaction between PES and hematite and it was concluded that there was only physical interaction between them.

**Table 3**
EDS results for polished surface of the composite at different regions.

| Region | Carbon (atomic %) | Oxygen (atomic %) | Iron (atomic %) | Silisium (atomic %) | Aluminum (atomic %) | Palladium (atomic %) |
|---|---|---|---|---|---|---|
| b1 | 78.37 | 14.80 | 4.38 | – | – | 2.45 |
| b2 | 28.07 | 33.54 | 35.69 | – | – | 2.70 |
| b3 | 19.78 | 42.13 | 7.65 | 26.90 | 1.42 | 2.12 |

### 4.2. IEMR attenuation performances of the composites

The determined values of the $\mu_L$, $\mu_M$ and HVL for the prepared composites and elemental lead (most widely used IEMR shielding material) are given in Table 4.

The $\mu_L$ values of the prepared composites showed a linear dependence on densities. This dependence is shown in Fig. 5 by plotting mean $\mu_L$ values for low (mean of 60, 88, 122, 166, 392 keV results), intermediate (mean of 662, 898 keV results) and high (mean of 1173, 1333, 1836 keV results) energy regions.

The interaction mechanisms of IEMR with matter differs due to energy of the IEMR. The predominant interaction process is proportional $Z^5$ for low, Z for intermediate and $Z^2$ for high IEMR energy regions (Friedlander et al., 1981). Thus increasing IEMR energy causes a decrement on the dependence of energy loss on Z of the absorber material. In the study, the $\mu_L$ values of the composites increased sharply with increasing density of the composites especially at low IEMR energy region, the density became ineffective on $\mu_L$ values for intermediate energy region and a slightly insignificant increasing behavior was observed for high energy region as expected (Fig. 5).

As a result of the same phenomena, the $\mu_L$ values of the composites with different filler loadings were found to decrease steeply with increasing IEMR energy at low energy region, while the filler loading increment caused a significant increment in $\mu_L$

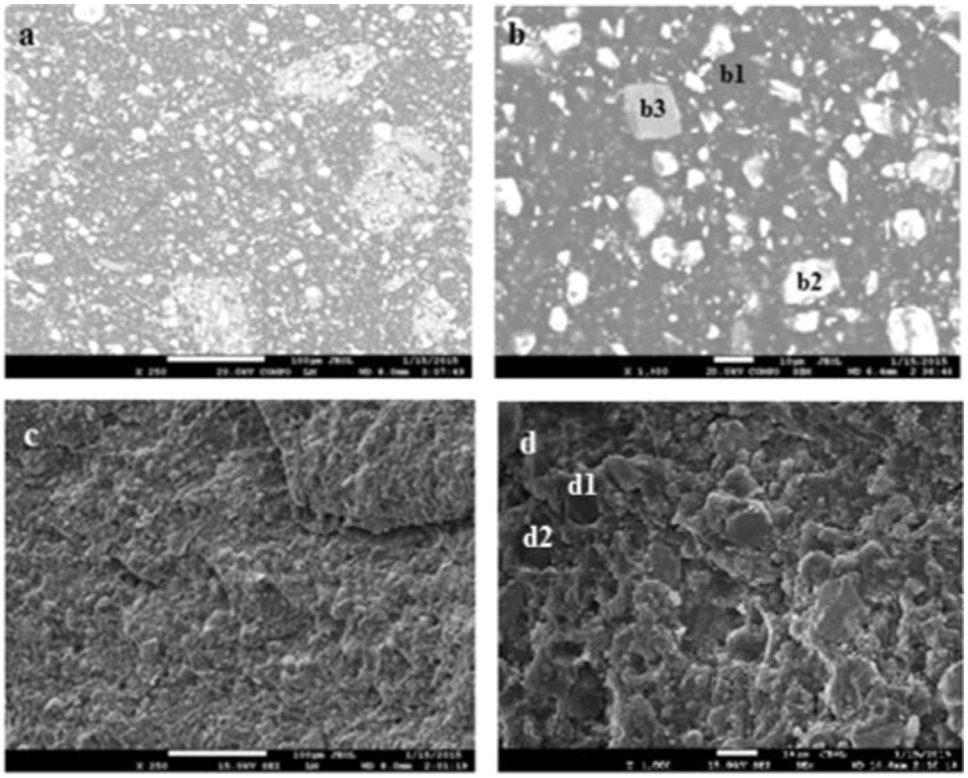


**Fig. 3.** SEM micrographs of HPES-50 for polished surface (a: x250, b: x1000) and fractured surface (c: x250, d: x1000).

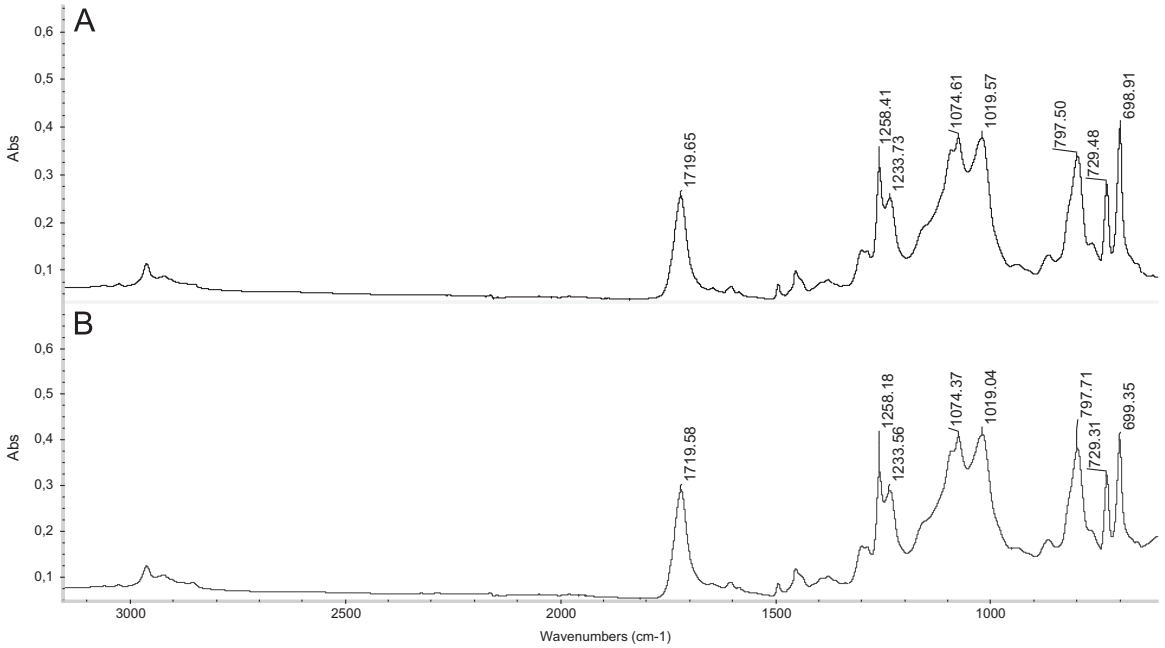


**Fig. 4.** FTIR spectrums of the PES (a) and HPES-50 (b).

**Table 4**
Determined $\mu_L$, $\mu_M$ and HVL values of the prepared composites and elemental lead.

| Sample designation | Low IEMR energy (keV) | | | | | Intermediate IEMR energy (keV) | | High IEMR energy (keV) | | |
|---|---|---|---|---|---|---|---|---|---|---|
| | 60 | 88 | 122 | 166 | 392 | 662 | 898 | 1173 | 1333 | 1836 |
| $\mu_L$ ($cm^{-1}$) | | | | | | | | | | |
| LEAD | 10.156 | 4.051 | 9.094 | 8.514 | 2.617 | 1.133 | 0.777 | 0.632 | 0.602 | 0.505 |
| HPES-10 | 0.340 | 0.320 | 0.280 | 0.340 | 0.200 | 0.140 | 0.090 | 0.120 | 0.070 | 0.040 |
| HPES-20 | 0.500 | 0.340 | 0.310 | 0.350 | 0.190 | 0.160 | 0.120 | 0.120 | 0.060 | 0.060 |
| HPES-30 | 0.660 | 0.500 | 0.320 | 0.370 | 0.200 | 0.170 | 0.120 | 0.130 | 0.100 | 0.100 |
| HPES-40 | 0.860 | 0.600 | 0.390 | 0.400 | 0.220 | 0.170 | 0.130 | 0.160 | 0.130 | 0.100 |
| HPES-50 | 1.170 | 0.740 | 0.450 | 0.410 | 0.230 | 0.190 | 0.150 | 0.160 | 0.150 | 0.100 |
| $\mu_M$ ($cm^2\ g^{-1}$) | | | | | | | | | | |
| LEAD | 0.896 | 0.357 | 0.802 | 0.751 | 0.231 | 0.100 | 0.069 | 0.056 | 0.053 | 0.045 |
| HPES-10 | 0.258 | 0.242 | 0.212 | 0.258 | 0.152 | 0.106 | 0.068 | 0.091 | 0.053 | 0.030 |
| HPES-20 | 0.350 | 0.238 | 0.217 | 0.245 | 0.133 | 0.112 | 0.084 | 0.084 | 0.042 | 0.042 |
| HPES-30 | 0.423 | 0.321 | 0.205 | 0.237 | 0.128 | 0.109 | 0.077 | 0.083 | 0.064 | 0.064 |
| HPES-40 | 0.497 | 0.347 | 0.225 | 0.231 | 0.127 | 0.098 | 0.075 | 0.092 | 0.075 | 0.058 |
| HPES-50 | 0.606 | 0.383 | 0.233 | 0.212 | 0.119 | 0.098 | 0.078 | 0.083 | 0.078 | 0.052 |
| HVL (cm) | | | | | | | | | | |
| LEAD | 0.068 | 0.171 | 0.076 | 0.081 | 0.265 | 0.611 | 0.892 | 1.096 | 1.151 | 1.372 |
| HPES-10 | 2.038 | 2.166 | 2.475 | 2.038 | 3.465 | 4.950 | 7.700 | 5.775 | 9.900 | 17.325 |
| HPES-20 | 1.386 | 2.038 | 2.235 | 1.980 | 3.647 | 4.331 | 5.775 | 5.775 | 11.550 | 11.550 |
| HPES-30 | 1.050 | 1.386 | 2.166 | 1.873 | 3.465 | 4.076 | 5.775 | 5.331 | 6.930 | 6.930 |
| HPES-40 | 0.806 | 1.155 | 1.777 | 1.733 | 3.150 | 4.076 | 5.331 | 4.331 | 5.331 | 6.930 |
| HPES-50 | 0.592 | 0.936 | 1.540 | 1.690 | 3.013 | 3.647 | 4.620 | 4.331 | 4.620 | 6.930 |

values. At the intermediate and high IEMR energy region the $\mu_L$ values were slightly decreased with increasing IEMR energy and the filler loading of the composites was nearly ineffective on IEMR attenuation performance of the shielding composite. In high energy region, the performances of some composites insignificantly increased with increasing photon energy and this can be attributed to several Compton scatterings beside the increasing interaction character of pair production (Fig. 6) (El-Sayed Abdo et al., 2003).

The $\mu_M$ values that represent attenuation per gram of materialof the prepared composites and elemental lead are also compared by using mean $\mu_M$ values for low, intermediate and high IEMR energy regions in Fig. 7.

The attenuation coefficients are also due to the molecular structure, binding characteristics and crystallographic structure of the absorber material especially for low energy region (El-Enany et al., 1994). In the study, although lead was approximately 10 times heavier than composites, incontestable lead had higher $\mu_M$ values than composites for low IEMR energies because of high dependence of predominant interaction mechanism of low energy photoelectric effect on interacting material's Z number. The closest packed crystal structure of the elemental lead that refers to a tightly packed and space efficient structure also had a significant effect on this result (Miessler and Tarr, 2004). In contrast, as the

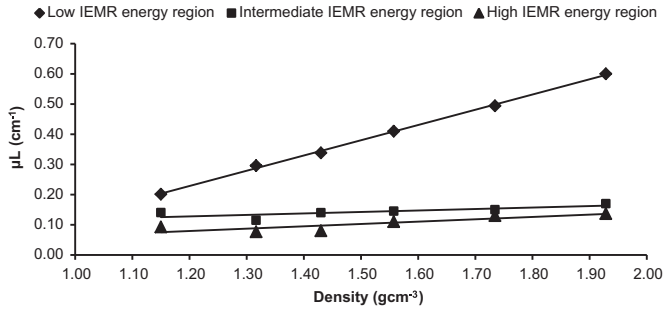


**Fig. 5.** Plot of linear dependence of $\mu_L$ values on density of hematite filled composites.

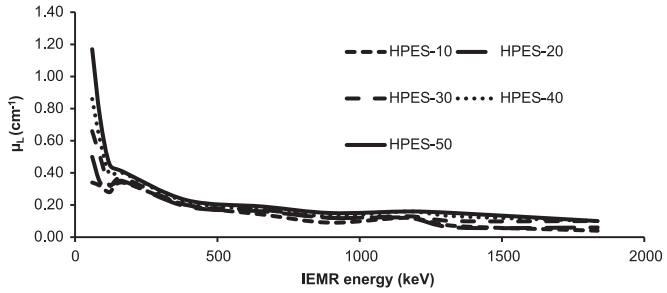


**Fig. 6.** $\mu_L$ values of the composites with respect to IEMR energy for different filler loadings between 0 and 2000 keV.

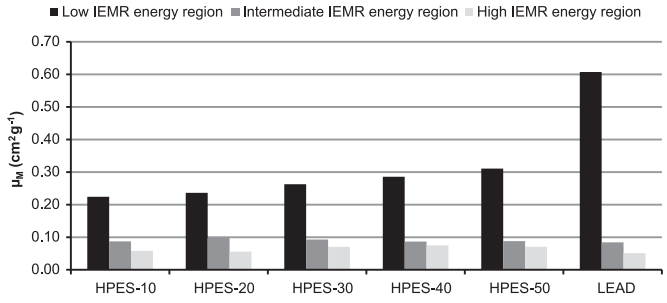


**Fig. 7.** $\mu_M$ values of the prepared composites and elemental lead.

**Table 5**
The comparison of $\mu_M$ values of various shielding materials reported in the literature.

| Shielding material | Reported $\mu_M$ ($cm^2\ g^{-1}$, 662 keV) |
|---|---|
| Lead | 0.100 (This study) |
| HPES-50 | 0.098 (This study) |
| Normal aggregate | 0.081 (Demir et al., 2011) |
| Barite | 0.076 (Demir et al., 2011) |
| Aluminium | 0.075 (LeClair, 2010) |
| Copper | 0.075 (LeClair, 2010) |
| 50% PbO + 50%$B_2O_3$ | 0.088 (Kirdsiri et al., 2009) |
| 85% Barite + 15% colemanite | 0.077 (Demir et al., 2011) |

IEMR energy increased dependence of attenuation on Z number decreased and the composite $\mu_M$ values became compatible with elemental lead. For the IEMR energies in the energy range of 500–1100 keV and $>1100$ keV all the hematite filled composites had higher $\mu_M$ values than elemental lead (Fig. 7).

The $\mu_M$ values of the prepared composites were compared with some other shielding materials reported in the literature in terms of 662 keV IEMR energy to find the shielding performances of the composites prepared in the study (Table 5). The 662 keV IEMR energy was chosen for comparison since it was the most widely studied energy in the literature.

Although it was an expected result that the low density of the composite matrix would reduce IEMR attenuation performance of the composites while providing lightness for the composite, the prepared composite with the best performance (HPES-50) provided $\mu_M$ value of elemental lead up to 98%. Also, HPES-50 was superior to normal aggregate, barite, aluminum, copper and other studied composites.

## 5. Conclusions

In the study, hematite particles were observed to disperse uniformly in the polymer matrix. PES based and hematite filled composites exhibited good IEMR shielding properties especially for high filler loadings. The density of the composites influenced the IEMR shielding performances of the composites for low IEMR energies but as the IEMR energy was raised the density effect on IEMR shielding performances became ineffective. The shielding performance parameter $\mu_M$ value of the composite with the best performance, HPES-50,reached 98% of elemental lead by being approximately 58% lighter. In addition, the studied composites were superior to lead because of the non-toxic nature of both matrix and filler materials.

## Acknowledgments

The authors would like to acknowledge the financial assistance of the Scientific and Technical Research Council of Turkey (TUBITAK) through Grant 213M323 December 2013 and Mugla Sitki Kocman University through the Grant 2014/003 February 2014.

## References

Demir, F., Budak, G., Sahin, R., Karabulut, A., Oltulu, M., Un, A., 2011. Determination of radiation attenuation coefficients of heavy-weight and normal-weight concretes containing barite for 0.663 MeV γ-rays. Ann. Nucl. Energy. 38, 1274–1278.
El-Enany, N., El-Kameesy, S.U., Miligy, Z., Ayad, M.A., Al-Kanawi, A.A., 1994. Practical study for the development of gamma rays shielding materials. Int. J. Environ. Stud. 46, 191–197.
El-Sarraf, M.A., El-Sayed Abdo, A., 2013. Influence of magnetite, ilmenite and boron carbide on radiation attenuation of polyester composites. Radiat. Phys. Chem. 88, 21–26.
El-Sayed Abdo, A., El-Sarraf, M.A., Gaber, F.A., 2003. Utilization of ilmenite/epoxy composite for neutrons and gamma rays attenuation. Ann. Nucl. Energy 30, 175–187.
Friedlander, G., Kennedy, J.W., Macias, E.S., Miller, J.M., 1981. Nuclear and Radiochemistry. John Wiley&Sons Inc., USA.
Gwaily, S.E., Madani, M., 2002. Lead-natural rubber composites as gamma radiation shields II: high concentration. Polym. Compos. 23, 495–499.
Harish, V., Nagaiah, N., Niranjana Prabhu, T., Varughese, K.T., 2008. Preparation and characterization of lead monoxide filled unsaturated polyester based polymer composites for gamma radiation shielding applications. J. Appl. Polym. Sci. 112, 1508–1530.
Kirdsiri, K., Kaewkhao, J., Pokaipisit, A., Chewpraditkul, W., Limsuwan, P., 2009. Utilization of ilmenite/epoxy composite for neutrons and gamma rays attenuation. Ann. Nucl. Energy 36, 1360–1365.
LeClair, P., 2010. Gamma Ray Attenuation. Available from ⟨http://faculty.mint.ua.edu/~pleclair/PH255/templates/formal/formal.pdf⟩.
Mheemeed, A.K., Hasan, H.I., Al-Jomaily, F.M., 2011. Gamma-ray absorption using rubber-lead mixtures as radiation protection shields. J. Radioanal. Nucl. Chem. 291, 653–659.
Miessler, G.L., Tarr, D.A., 2004. Inorganic Chemistry. High Education Press, Chineese.
Plionis, A.A., Garcia, S.R., Gonzales, E.R., Porterfield, D.R., Peterson, D.S., 2009. Replacement of lead bricks with non-hazardous polymer-bishmuth for low-energy gamma shielding. J. Radioanal. Nucl. Chem. 282, 239–242.
Settle, F., 1997. Handbook of Instrumental Techniques for Analytical Chemistry. Prentice Hall PTR, New Jersey.
Kansouh, W.A., 2012. Radiation distrubition through serpentine concrete using local materials and its application as a reactor biological shielding. Ann. Nucl. Energy 47, 258–263.
Bashter, I.I., Makarious, A.S., El-Sayed Abdo, A., 1996. Investigation of hematite-serpentine and ilmenite–limonite concretes for reactor radiation shielding. Ann. Nucl. Energy 23, 65–71.